

# NUMERICAL OPTIMISATION OF ADAPTIVE TRANSONIC AIRFOILS WITH VARIABLE CAMBER

**Andreas Sommerer , Thorsten Lutz , Siegfried Wagner**  
**Institute for Aerodynamics and Gas Dynamics, University of Stuttgart, Germany**

**Keywords:** *Numerical Optimisation, Transonic Flow, Shock Control Bump, Variable Camber, Adaptive Wing*

## Abstract

*A special research group (SFB 409) has been established at Stuttgart University to investigate the potential of adaptive structures for aerospace application.*

*One project deals with concepts and aerodynamics of adaptive transonic wings. To cope with the problem of flight at transonic Mach numbers adaptive mechanisms are introduced. Aerodynamic efficiency at off-design conditions is improved by the application of a shock control bump (SCB) on a variable camber (VC) airfoil. Since a SCB has to be properly shaped and positioned to generate a favourable effect, relevant geometrical parameters were investigated using direct numerical optimisation. An optimisation environment was developed consisting of a hybrid optimiser, a geometry module and a coupled Euler boundary-layer code. For a specified off-design condition bump shapes were optimised, while the influence of various geometric bump representations was investigated. Shape optimisations for an adaptive bump were carried out for different Mach numbers at a fixed lift coefficient. To overcome the problem of narrow Mach regions of significant drag reduction for one-point designed bumps, multi-point designs were performed. Finally a VC-SCB combination was numerically optimised in order to improve the performance for several off-design conditions.*

## 1 Introduction

A permanent goal for modern aircraft technologies is the reduction of DOCs by reducing fuel consumption and increasing mission flexibility. As these goals are strongly related to the aerodynamic efficiency of the wing it is necessary to optimise the wing performance. A conventional approach is aimed to show a good performance within a certain range of flight conditions. However, the performance in each single point of the cruise envelope does not represent an optimum. For flight conditions outside that region caused for example by a weight change because of fuel consumption aerodynamic efficiency decreases considerably.

A possibility to cope with that problem is the adaption of the wing geometry. The practical application of real-time adaptive configuration optimisation for enhanced transport performance on an L-1011 Tristar aircraft was investigated by Gilyard et al. [11]. A variable camber (VC) mechanism was established using the outboard ailerons. Evans et al. [9] describe the utilisation of the capabilities of an advanced wing technology to an experimental F-111 fighter. This so-called Mission Adaptive Wing includes leading and trailing edge variable camber mechanisms for an improved manoeuvrability and performance. Austin et al. [2] suggest a wing which allows the adaption of the complete wing section. A complex system of actuators was integrated into a demonstrator in order to realize active ribs that reshape the wing section by deform-

ing the structure. In 1992, Ashill et al. [1] proposed a concept that limits the geometry adaption to a small segment on the suction side of the airfoil. To cope with the strong shock-waves near the end of the laminar section on NLF-airfoils a bump was introduced to reduce wave-drag. The so-called Shock Control Bump (SCB) in combination with a VC-mechanism is subject to the present investigations.

After a brief introduction to the fundamentals of the bump, the aerodynamic calculation codes applied are briefly described. Following an explanation of the optimisation environment, different bump shapes are designed by means of numerical optimisation. From these results, investigations on the potential of an adaptive bump and a multi-point designed bump are deduced. Finally combined VC-SCB optimisations are carried out to generate a superior  $\frac{L}{D}$  envelope for an airfoil at off-design conditions.

## 2 Fundamentals of the Shock Control Bump

One major challenge for airliners is flight at transonic Mach numbers. If the critical Mach number is exceeded locally supersonic regions and shock waves appear on the airfoil. Through the shock, entropy is increased in the flow-field while total pressure is decreased. The resulting pressure drag is called wave drag which is responsible for the transonic drag rise.

To deal with this problem, supercritical airfoil designs are applied which show a shock-free pressure distribution in their design point, thereby avoiding wave-drag. The supersonic flow is decelerated to subsonic Mach numbers without a shock by isentropic compression waves. However, for a fixed geometry this supercritical behaviour is limited to a narrow region of flight conditions.

The SCB maps the mechanism of deceleration by the isentropic compression waves on a smaller scale, i. e. the effective region is limited to 20% ÷ 25% of the chord length. On the concave part of the upstream side of the bump isentropic compression waves are induced leading to a pre-shock compression and thus decrease

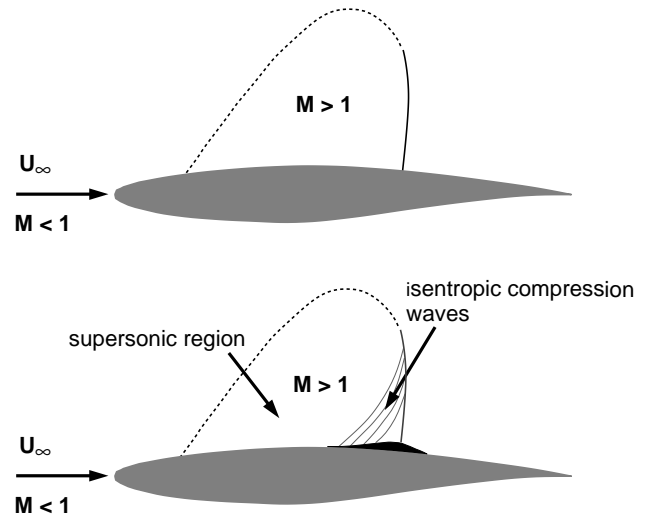


Fig. 1 Principle of the shock control bump.

the Mach number in front of the shock. Further downstream the flow is decelerated to subsonic Mach numbers via a significantly reduced shock. Fig. 1 illustrates the effect of a well shaped and positioned bump, while the corresponding  $c_p$  distribution is depicted in Fig. 2.

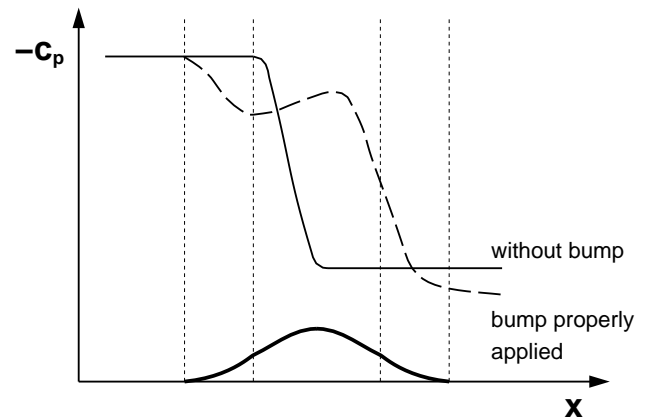
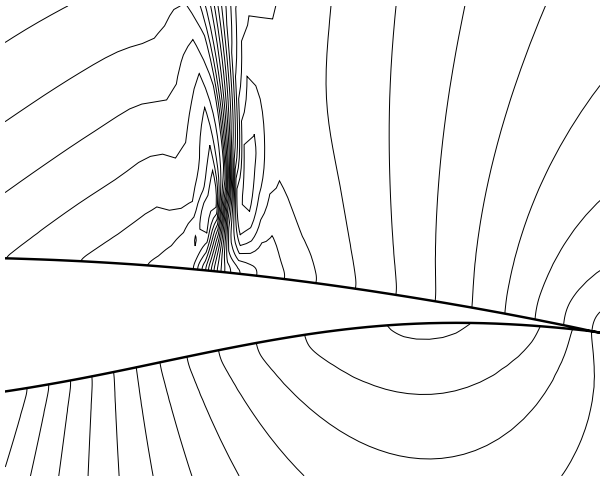
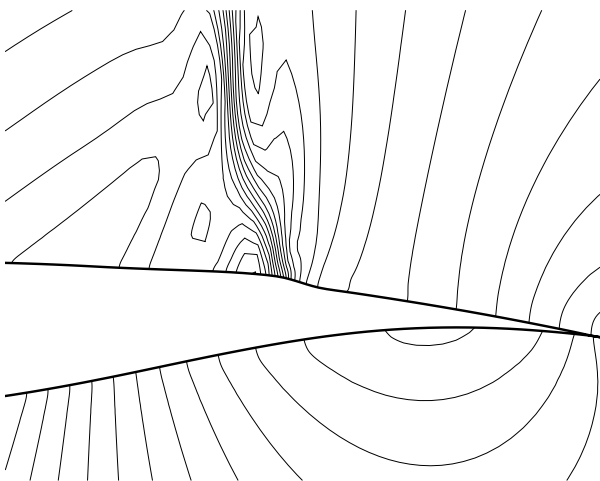


Fig. 2 Pressure distribution for a properly positioned and shaped bump.

Fig. 3 and 4 show isobars of the shockwave region of a DA VA2 airfoil [6] as calculated with the Navier-Stokes-Code MUFLO (see section 3.2) for the clean and a bump added geometry respectively. One can see that in comparison to the clean airfoil the shock is shifted downstream while the isobars are spread by the bump.



**Fig. 3** Isobars in the shock region of a DA VA2 airfoil at  $M_\infty = 0.77$  and  $c_l = 0.524$  (result MUFLO).



**Fig. 4** Isobars in the shock region of a DA VA2 airfoil with an optimised SCB applied at  $M_\infty = 0.77$  and  $c_l = 0.524$  (result MUFLO).

This means the pressure gradients are reduced which results in lower wave drag. Similar to the supercritical airfoil, the SCB has a design point as well as an off-design region. Improperly placed or shaped bumps lead to double shock systems or boundary-layer separation.

Up to now several parametrical investigations have been carried out dealing with the accurate shaping and positioning of the shock control bump. Gildemeister et al. [10] and Knauer [15]

investigated bump families with the general shape of a loaded beam with different positions, heights and asymmetries. They showed that with increasing off-design Mach number or lift coefficient the height of the bump has to be increased. Maximum suggestive bump heights amount to about 0.5% of the airfoil chord length. Dargel [4, 5] extended these investigations to other bump shapes like ramps, polynomials and sinusoidal curves. He found that in contrast to the bump height and position the detailed bump shape does not have a very strong impact on the drag reduction effect. According to the research performed in the EUROSHOCK-program [16, 17] the SCB is the most effective shock control system of the mechanisms investigated.

### 3 Aerodynamic Model

#### 3.1 MSES

For application in the optimisation environment the MSES code by M. Drela [7, 8] was chosen for the aerodynamic analysis. This 2D-Euler code is coupled with an integral boundary-layer method. Because of the huge amount of calculations to be carried out for an optimisation process it is necessary to choose a highly efficient code. MSES is convincing in this respect and also because of its good accuracy and robustness. The Euler equations are solved on a streamline adapted mesh. As a consequence the position of the mesh points is subject to the iteration process on the way to a converged solution. With the application of that technique diffusion between adjacent streamlines is eliminated resulting in a completely non-dissipative scheme in subsonic regions with the benefit that drag evaluation can be carried out by the evaluation of the entropy and the momentum at the outflow boundary. The calculation of viscous effects is based on numerical integration of the integral momentum and energy equation utilising Green's lag equation to determine the dissipation coefficient for turbulent flows. MSES calculations can be carried out for forced and free transition. For all the optimisations discussed in the present paper the transition

location was fixed.

### 3.2 MUFLO

To verify the optimisation results the 2D Navier-Stokes solver MUFLO developed by W. Haase [12, 14] was used. The governing equations are solved with a Jameson type cell-centred finite-volume scheme. Numerical stability is achieved by adding a blend of second and fourth differences in the flow variables to the convective and diffusive fluxes. Viscous fluxes are implemented by central differences of second order. The time integration to steady state is done by means of a fully explicit five-stage hybrid time-stepping scheme of Runge-Kutta type. In order to accelerate convergence a local time-stepping scheme is applied determining the maximum permissible time step for every cell by local stability analysis. To add implicit character to the problem and thus increasing the CFL number implicit residual smoothing is applied. A multi-grid scheme implemented for further convergence acceleration uses either a V or a W cycle. From several turbulence models available, the Johnson-Coakley model was chosen for the present calculations. According to [13] it is assumed to yield reliable results in the presence of shocks.

## 4 Numerical Optimisation

Numerical optimisation techniques become more and more important in nowadays design processes. While they cannot replace the experience of an engineer, they offer ways to unconventional solutions and thus are a well suited supplementary design tool.

Depending on the complexity of the optimisation problem the topology of the objective function sets up the challenge for the numerical optimiser. Smooth, uni-modal topologies can be easily treated by gradient methods, while complex multi-modal topologies, that can consist of narrow valleys, large plains or even holes and singularities make the use of alternative strategies like Genetic Algorithms or Evolution Strategies indispensable.

For the present investigations an optimisation environment was developed. The Pointer Code of Synaps [18] represents the numerical optimisation module. This hybrid optimiser consists of a Genetic Algorithm, a Downhill Simplex and a Gradient Method module. During the optimisation run Pointer utilises a mix of these algorithms. For particular tasks proper optimiser compositions can be "trained".

In setting up the optimisation task, the user provides the optimiser with a set of design variables, appropriate constraints as well as an initial geometry. The values for the design variables are chosen by the optimiser and transferred into an iterative process in order to minimise the objective function value. With the current set of design variables, the geometry module generates a modified mesh. This new mesh is subject to the aerodynamic calculation performed by the analysis module. The calculated values of the objective function and the constraints are given back to the optimiser that generates a new set of design variable values. The process is terminated if no further improvement can be found or if a prescribed time limit is reached.

## 5 Results and Discussion

In the following sections the optimisation environment is applied in the investigation of adaptive mechanisms for the DA VA2 as well as the ONERA OAT15A [3] airfoil at moderate off-design conditions. The DA VA2 airfoil is used as a basic airfoil for the SCB optimisations. It shows a turbulent type pressure-distribution and was designed for the following conditions:

$$M = 0.73, \quad c_l = 0.524, \quad Re = 1.0 \cdot 10^7 \quad (1)$$

The OAT15A section serves as a basic airfoil for the combined VC-SCB investigations. This airfoil shows the following design conditions:

$$M = 0.705, \quad c_l = 0.75, \quad Re = 1.6 \cdot 10^7 \quad (2)$$

### 5.1 Bump Parametrisation

Before performing a combined VC-SCB optimisation a suitable bump representation was inves-

tigated. The effort needed to treat an optimisation problem depends on the efficiency of the aerodynamic analysis code, the topology of the objective function, the utilised optimisation algorithm as well as the number of design variables. The number of calculations to be carried out on the way to the optimum is increased disproportionately with additional design variables. Because of the time consuming analysis coming along with complex aerodynamic problems it is necessary to minimise the number of design variables. This leads to different parametrisation techniques and thus shape families. For the current investigations the adaptable segment of the airfoil was fixed to 20% of the chord length. Different parametrisations were applied and investigated with respect to the influence on wave drag and viscous drag behaviour.

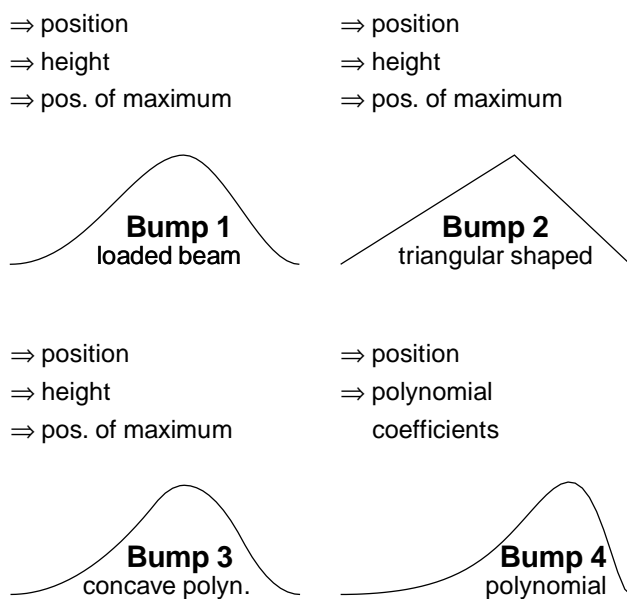


**Fig. 5** Investigated bump shapes with corresponding design variables.

Alternative representations of bump shapes along with the necessary design variables are shown in Fig. 5. The functional value at a position  $x$  of these approaches is added to the airfoil geometry in wall normal direction. The manifold of the educible shapes is determined by the number of design variables. Thus a polynomial bump represented by 12 coefficients enables a more detailed manipulation of the pressure distribution.

Bump 1 was subject to previous investigations [10, 15]. It shows the contour of a beam fixed on either side under the load of a linearly varying force distribution. Its shape is determined by prescribing the length, height and the relative position of the maximum. The bump does not yield contour discontinuities at the joints to the basic airfoil. Bump 2 is a triangle-shaped geometry, which does not fulfill tangential conditions at its edges and introduces a kink at its maximum. Bump 3 consists of a set of four polynomial segments. They are designed in a manner that the point of inflection on the upstream flank of the bump is placed to be very close to the bump maximum providing the geometry with a long concave region. The idea is that the isentropic compression waves that weaken the shock (see also section 2) emanate from the concave part of the bump geometry. The special design of bump 3 reduces the acceleration of the flow in the now shorter segment of convexity after the compression on the concave part. Bump shape 4 was designed to provide the optimiser with a big variety of shapes. It is set up by a polynomial of 11th order.

$$c(x) = \sum_{i=0}^{11} a_i \cdot x^i \quad (3)$$

Four coefficients are set in order to fulfill the boundary conditions of the geometry i. e. vanishing height and gradient at the edges. This leaves 8 coefficients as design variables  $a_2 \dots a_9$  to be modified by the optimiser. A drawback of that geometry representation is that compared to the previous shape families there is much more effort for the optimisation involved. However since the range of possible geometries is increased statements can be made if there is more drag reduction potential than that offered by the simple three-parameter designs.

## 5.2 One-Point Design

To investigate the wave drag reduction potential of the SCB, onset flow conditions were chosen which are noticeably out of the design-region of the basic airfoil. The bumps were optimised for a design condition of  $M = 0.77$ ,  $c_l = 0.524$

and  $Re = 1.0 \cdot 10^7$ , corresponding to the design lift coefficient of the DA VA2 airfoil at an increased Mach number. Transition was fixed at 10% chord length. Fig. 6 depicts relative gains in wave drag, viscous drag and total drag for the optimised bump shapes according to the different parametrisations.

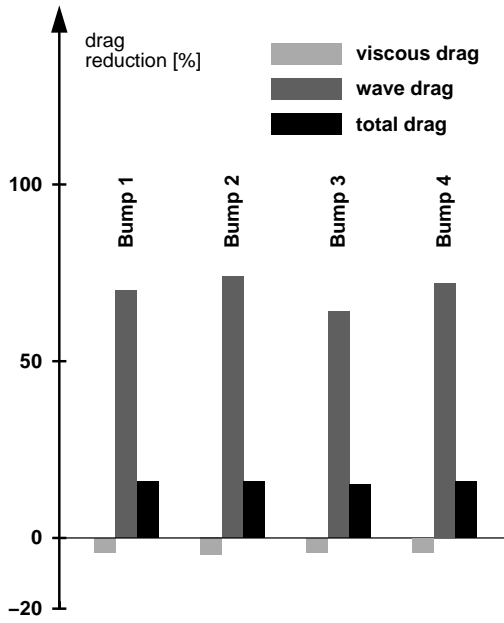


**Fig. 6** Components of drag gain for different bump shapes at a design point of  $M = 0.77$  and  $c_l = 0.524$  (basic airfoil DA VA2, result MSES).

It is obvious that the maximum achievable drag reduction is almost identical for all basic bump shapes. The 8-parameter polynomial bump (bump 4) together with bump 2 shows the best performance while all other shapes are just slightly inferior. The relative reduction of wave drag for all bump shapes is impressive, however, it is accompanied by an increased viscous drag. The reduction of the total drag for the considered off-design condition for all bumps was found to be about 16%.

Pressure distributions for the clean airfoil and the optimised bumps are depicted in Figs. 7 and 8. The magnified shock region shows that bump 1 to 4 influence the pressure distribution in different ways despite the drag reduction is almost identical. With the exception of bump 3 all other

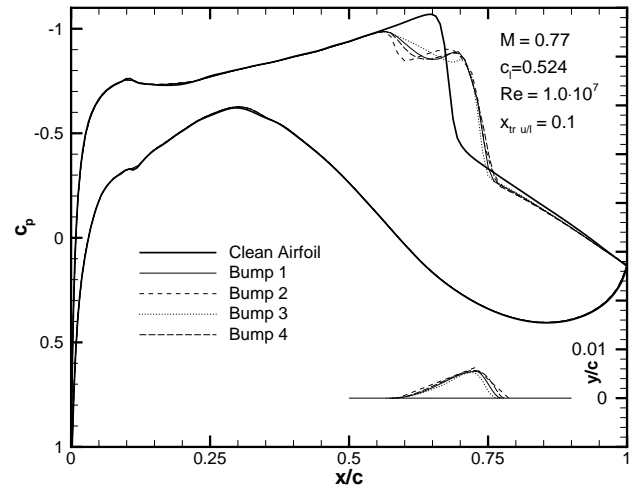


**Fig. 7** Pressure distribution for different optimised bumps with corresponding bump geometries (result MSES).

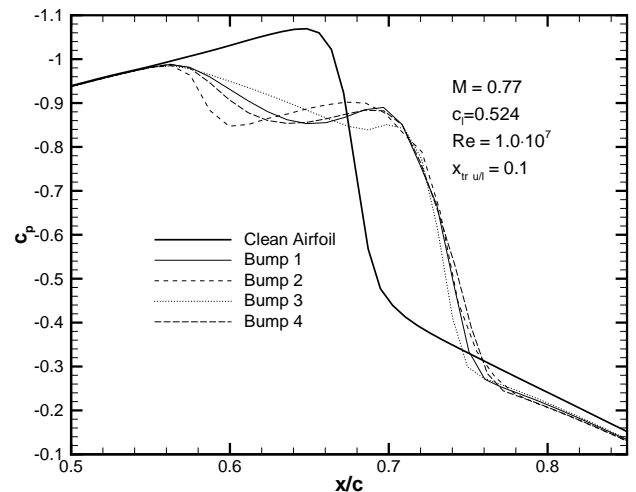


**Fig. 8** Magnified shock region.

SCBs show flow acceleration immediately upstream of the shock. Bump 3 does not cause an acceleration because of the small convex segment on the upstream flank. Regarding the optimised bump geometries in Fig. 7 it is noticeable that the characteristic geometric parameters for an SCB like height, position and asymmetry are very similar.

In the off-design region of the SCBs additional drag is introduced visualised by the drag polars in Fig. 9. Validation calculations for the optimised bump shape 1 were performed by means of the MUFLO code and are marked with

circle symbols. Within the design region of the SCB an excellent correspondence to the MSES results is recognisable.

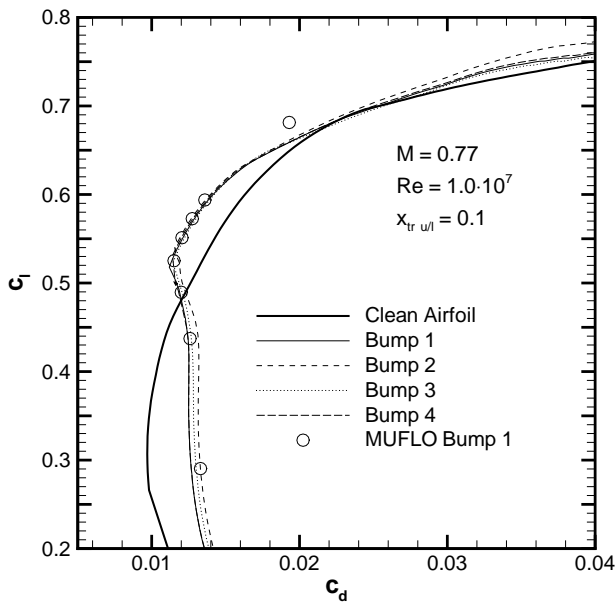


**Fig. 9** Drag polars for the clean airfoil and different bump shapes at the design Mach number of the bumps (result MSES and MUFLO).

In Fig. 10 the design Mach number of the bumps is clearly indicated by a narrow valley. Outside of the design point the bumps cause an increased drag coefficient compared to the clean airfoil. Especially at Mach numbers below the design Mach number of the bump, the drag characteristics are worsened while at higher Mach numbers the bump is still favourable within a certain range. Because of the negligible differences in performance between the different parametrisations, bump shape 1 was chosen for further investigations. With only three design parameters it minimises optimisation effort.

The narrow drag optimum makes a static bump useless for practical application on an aircraft wing. The bump must be adapted to the current flight conditions. Operated outside of its design region the bump can deteriorate the airfoil performance. A bump positioned too far downstream does not effect the shockwave. Downstream of the shock the flow accelerates again along the upstream flank of the bump. Then

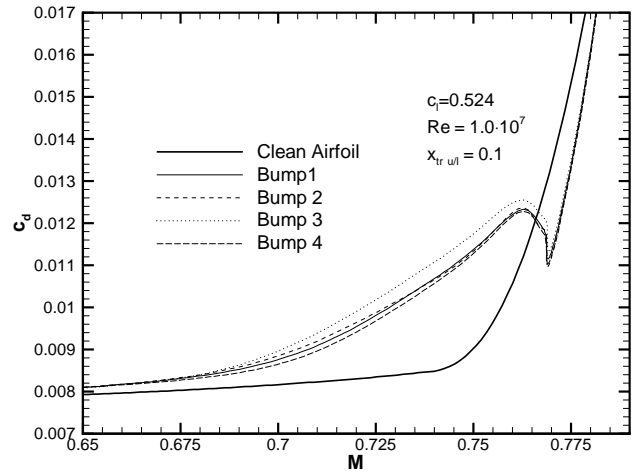


**Fig. 10** Mach-polars for the clean airfoil and different bump shapes at the design lift coefficient of the bumps  $c_l = 0.524$  (result MSES).

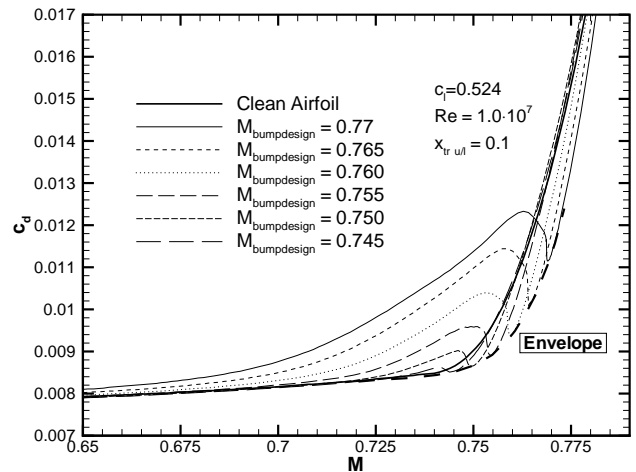


**Fig. 11** Envelope of an adapted bump compared to the clean airfoil (result MSES).

following a second supersonic region another shockwave is to be found. It is obvious that such a double shock configuration produces more drag than the clean airfoil at the same flight condition.

A mechanism providing the airfoil continuously with the proper bump shape and position yields an improved aerodynamic efficiency in the whole off-design region of the basic airfoil. Several optimised bumps for different design Mach numbers are illustrated in Fig. 11. It is clear to see that the envelope of all the corresponding design points is shifting the drag rise to higher Mach

numbers, thus improving the aerodynamic capability of the airfoil.

### 5.3 Multi-Point Design

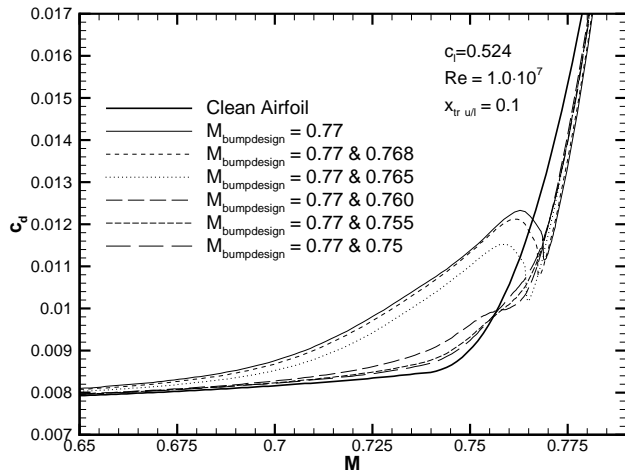


**Fig. 12** Multi-point optimisation for different regions of  $\Delta M_{design}$  (result MSES).

Determination of the exact flight condition in real flight represents a sophisticated task. Thus it is anticipated that SCBs for practical use must yield a reduced sensitivity to small changes of the onset flow. Because of the narrow Mach region of reduced drag coefficients for a one-point designed SCB multi-point designs were introduced. The objective function for the multi-point optimisation is changed to be represented by the sum of two drag coefficients at two different Mach numbers. Fig. 12 shows  $c_d$  vs.  $M$  for several two-point optimised bumps. Since no weighting factors were involved in the optimisation process, the lower edge of the Mach-region implicitly has a lower priority than the upper edge since it introduces less wave drag that can be reduced. Thus the bump optimised for the most extended region of  $\Delta M = 0.02$  even shows a higher drag coefficient for the lower design Mach number compared to the clean airfoil while being favourable in the remaining design region. However, it can be stated that at the cost of less maximum drag reduction the region in which the bump is effective is broadened.

### 5.4 Combined VC-SCB Optimisation

While flying at high lift coefficients a VC mechanism proves to be advantageous regarding the maximum  $\frac{L}{D}$ . Caused by an increased camber the corresponding angle of attack for a certain lift coefficient is reduced. This leads to a changed circulation distribution with the benefit of a lower suction peak in the nose region. In the transonic flow regime the induced reduction of pre-shock Mach number weakens the shock strength thus reducing wave drag. For off-design flight conditions a significant improvement of the aerodynamic efficiency can be achieved. Fig. 13 illustrates the  $\frac{L}{D}$  curves of the OAT15A airfoil for several flap deflection angles. The envelope for the VC-airfoil (dashed line) clearly shows an improvement compared to the clean airfoil.

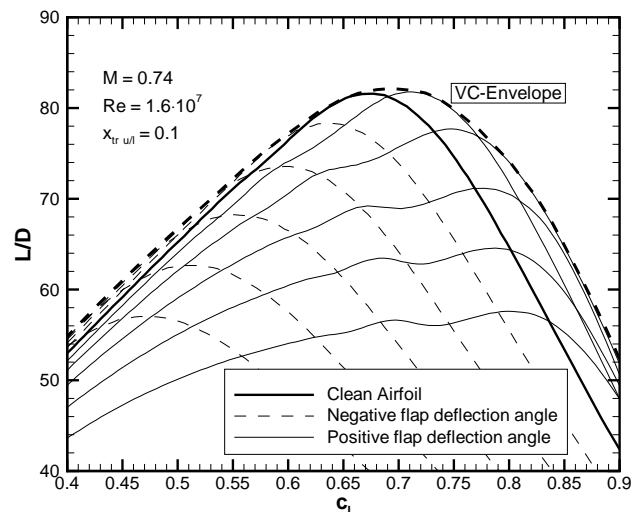


**Fig. 13**  $\frac{L}{D}$  vs.  $c_l$  for the ONERA OAT15A airfoil at  $M = 0.74$  with different flap deflection angles (result MSES).

Because of its wave drag reducing capability an additionally applied bump promises a further increase of the aerodynamic efficiency. Direct numerical optimisations for a VC-SCB combination were carried out in order to estimate the additional improvement. The SCB was modelled by three design variables according to bump shape 1 (see also Sec. 5.1). The flap hinge was centred at 80% chord length. The flap deflection angle

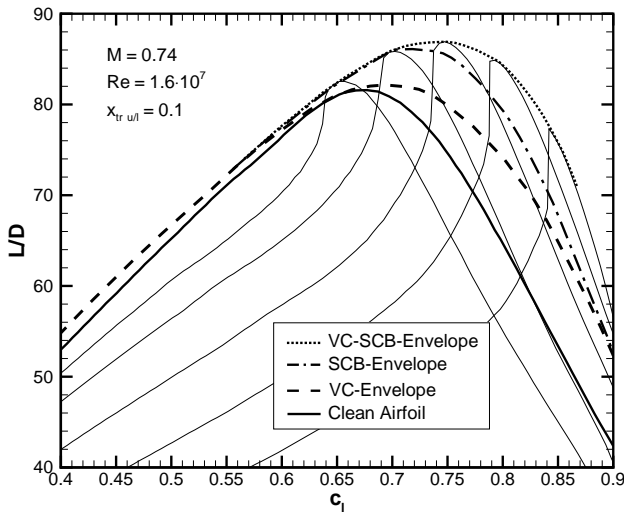


**Fig. 14**  $\frac{L}{D}$  vs.  $c_l$  for the ONERA OAT15A airfoil at  $M = 0.74$  for several optimised VC-SCB combinations (result MSES).

represented the fourth design variable. Fig. 14 depicts the lift to drag ratio plotted against the lift coefficient for the clean airfoil, the envelope of the VC-airfoil (dashed line) as well as the envelope of the VC-SCB combination (dotted line). Significant additional gains for the combination are visible. Supplementary the optimised lift to drag ratio for the adaptive SCB only airfoil is depicted (dash-dot line) showing an envelope between the VC and the VC-SCB mechanism. Investigations of the resulting optimised bump geometries of the VC-SCB combination show a noticeably reduced bump height compared to the optimised SCB only geometry.

## 6 Concluding Remarks

Investigations regarding the application of shock control bumps as well as VC-SCB combinations on transonic airfoils were presented. In order to compare the drag reduction potential of several SCB shapes numerical optimisations were performed. Beside one-point optimisations for different Mach numbers several multi-point optimisation for Mach regions up to  $\Delta M = 0.02$  were carried out. To improve aerodynamic efficiency at higher lift coefficients a combined VC-SCB

approach was optimised for several off-design conditions.

The calculated results show an encouraging potential for the application of the SCB on a transonic airfoil. With the reduction of wave drag in the off-design region the flight Mach number can be increased for a given  $c_l$ . The detailed shape of the SCB has turned out to be of minor importance while bump position, height and the location of the bump maximum play a major role. With an increasing width of the design Mach number regime the favourable effect on wave drag is reduced. The envelope of several optimised bumps shows the advantages of an adaptive bump. The VC-SCB combination yields a significantly improved lift to drag ratio in its design region compared to the clean airfoil as well as to the VC airfoil.

Wind tunnel tests to be performed in the transonic wind tunnel of Munich are being prepared in order to validate the present theoretical results. To check the possibilities of bump application on a wing the on-going investigations are planned to be extended to 3D wings in the near future.

## 7 Acknowledgements

The authors thank M. Drela of MIT for providing MSES that is part of the present optimisation environment as well as W. Haase of DASA for making the MUFLO Code available that allowed a validation of the optimised geometries. This research was supported by the German Research Foundation (DFG).

## References

- [1] Ashill P. R., Fulker J. L. and Shires A. A novel technique for controlling shock strength of laminar-flow aerofoil sections. *Proceedings 1st European Forum on Laminar Flow Technology, March 16–18, 1992, Hamburg, Germany*, pp 175–183. DGLR, AAAF, RAeS, 1992.
- [2] Austin F., Rossi M. J., Nostrand W. V., Knowles G. and Jameson A. Static shape control for adaptive wings. Vol. 32, No 9, September 1994.
- [3] Bezar H. Personal Correspondence. ONERA.

- [4] Dargel G. Widerstandsreduktion durch Stoßkontrolle mit adaptiver Hautstruktur: Shock Control Bump. *Proceedings DGLR Jahrestagung*, 1998.
- [5] Dargel G. and Archambaud J. P. Assessment of the capability of drag reduction of the shock control device sc bump on airfoil flows and application aspects on wing. *Proceedings IUTAM Symposium on Mechanics of Passive and Active Flow Control, 7–11 September, 1998, Göttingen, Germany*, pp 57–62. Kluwer Academic Publishers, 1998.
- [6] Dargel G. Personal Correspondence. DASA, Bremen.
- [7] Drela M. Two-dimensional transonic aerodynamic design and analysis using the euler equation. Report No. 187, MIT Gas Turbine & Plasma Dynamics Laboratory, 1986.
- [8] Drela M. and Giles M. B. Ises: A two-dimensional viscous aerodynamic design and analysis code. AIAA 25th Aerospace Sciences Meeting, January 12-15, 1987, Reno, Nevada, USA; also: AIAA-86-0424.
- [9] Evans M. R., Hynes R. J., Norman D. C. and Thomasson R. E. Automatic flight control modes for the AFTI/F-111 mission adaptive wing aircraft. AGARD-CP-384, Vol. 25 (1984).
- [10] Gildemeister L., Dargel G. and Hansen H. Theoretische Grundsatzuntersuchungen zum Thema 'Adaptive Hautstrukturen im Verdichtungsstoßbereich'. *DGLR Fachausschußtagung T 2.2 "Experimentelle Aerodynamik", 2./3. Mai 1996, Technische Universität Berlin*, pp 69–78, May 1996.
- [11] Gilyard G. B., Georgie J. and Barnicki J. S. Flight test of an adaptive configuration optimization system for transport aircraft. Technical Report NASA/TM-1999-206569, NASA, Dryden Flight Research Center Edwards, California 93523-0273, January 1999.
- [12] Haase W., Wagner B. and Jameson A. Development of a navier-stokes method based on a finite volume technique for the unsteady euler equations. *Proceedings of the 5th GAMM-Conference on Numerical Methods in Fluid Mechanics, October 5–7, 1983, Rome, Italy*, pp 99–107. Friedrich Vieweg & Sohn, Braunschweig, Germany, 1983.
- [13] Haase W., Chaput E., Elsholz E., Leschziner M. A. and Müller U. R., editors. *Validation of CFD Codes and Assessment of Turbulence Models*. Vol. 58 of *Notes on Numerical Fluid Mechanics*, Friedrich Vieweg & Sohn Verlagsgesellschaft mbH, Braunschweig/Wiesbaden, 1997. ISBN 3-528-06958-9.
- [14] Jameson A., Schmidt W. and Turkel E. Numerical solution of the euler equations by finite volume methods using runge kutta time stepping schemes. *Proceedings 14th Fluid and Plasma Dynamics Conference, June 23–25, 1981, Palo Alto, USA*. AIAA, 1981. Proceedings of a symposium held at NASA Langley Research Center, Hampton, Virginia, March 29–30, 1979.
- [15] Knauer A. *Die Leistungsverbesserung transsonischer Profile durch Konturmodifikationen im Stoßbereich*. PhD thesis, DLR, 1998.
- [16] Stanewski E. Euroshock I and II: A survey. *Proceedings IUTAM Symposium on Mechanics of Passive and Active Flow Control, 7–11 September, 1998, Göttingen, Germany*, pp 35–42. Kluwer Academic Publishers, 1998.
- [17] Stanewsky E., Fulker J., Delery J. and Geissler J. *Drag Reduction by passive Shock Control - Results of the Project EUROSHOCK, AER2-CT92-0049*. Vol. 56 of *Notes on Numerical Fluid Mechanics*, Vieweg Verlag, 1997.
- [18] Synaps Inc. *Pointer Optimization Software Release 1.3 User's Guide*. 970 Sidney Marcus Boulevard, Suite 2302, Atlanta, GA 30324, USA., 1998.